

GA-A26565

LIMITS TO H-MODE PEDESTAL PRESSURE GRADIENT IN DIII-D

by

R.J. GROEBNER, P.B. SNYDER, T.H. OSBORNE, A.W. LEONARD,
T.L. RHODES, L. ZENG, E.A. UNTERBERG, Z. YAN, G.R. McKEE,
C.J. LASNIER, J.A. BOEDO,[†] and J.G. WATKINS

OCTOBER 2009



DISCLAIMER

This report was prepared as an account of work sponsored by an agency of the United States Government. Neither the United States Government nor any agency thereof, nor any of their employees, makes any warranty, express or implied, or assumes any legal liability or responsibility for the accuracy, completeness, or usefulness of any information, apparatus, product, or process disclosed, or represents that its use would not infringe privately owned rights. Reference herein to any specific commercial product, process, or service by trade name, trademark, manufacturer, or otherwise, does not necessarily constitute or imply its endorsement, recommendation, or favoring by the United States Government or any agency thereof. The views and opinions of authors expressed herein do not necessarily state or reflect those of the United States Government or any agency thereof.

LIMITS TO H-MODE PEDESTAL PRESSURE GRADIENT IN DIII-D

by

R.J. GROEBNER¹, P.B. SNYDER¹, T.H. OSBORNE¹, A.W. LEONARD¹,
T.L. RHODES², L. ZENG², E.A. UNTERBERG³, Z. YAN⁴, G.R. McKEE⁴,
C.J. LASNIER⁵, J.A. BOEDO^{6,†} and J.G. WATKINS⁷

This is a preprint of a paper to be presented at the 12th International Workshop on H-Mode Physics and Transport Barriers, September 30 Through October 2, 2009, in Princeton, New Jersey, and to be published in a special issue of *Nuclear Fusion*.

¹General Atomics, P.O. Box 85608, San Diego, California, USA.

²University of California-Los Angeles, Los Angeles, California, USA

³Oak Ridge National Laboratory, Oak Ridge, Tennessee, USA

⁴University of Wisconsin-Madison, Madison, Wisconsin, USA

⁵Lawrence Livermore National Laboratory, Livermore, California, USA

⁶University of California-San Diego, La Jolla, California, USA

⁷Sandia National Laboratories, Albuquerque, New Mexico, USA

Work supported by
the U.S. Department of Energy
under DE-FC02-04ER54698, DE-FG02-08ER54984, DE-AC05-00OR22725,
DE-FG02-89ER53296, DE-FG02-08ER54999, DE-AC52-07NA27344,
DE-FG02-07ER54917, and DE-AC04-94AL85000

GENERAL ATOMICS PROJECT 30200
OCTOBER 2009



1. ABSTRACT

The spatial and temporal evolution of the total pedestal pressure profile has been measured during the pedestal evolution between successive edge localized modes (ELMs) of Type I ELMing H-mode discharges in DIII-D. Measurements are used to test a model that predicts that kinetic ballooning modes provide a strong constraint on the pedestal pressure gradient obtained during an inter-ELM cycle and cause the pedestal width to scale as the square root of the pedestal poloidal beta. Discharges in two different parameter regimes are examined for evidence that the evolution of the pressure gradient reaches a limit prior to the onset of an ELM. Both discharges show evidence of rapid evolution of the pressure profile very early in the recovery phase from an ELM. In one discharge, the pressure gradient reached approximate steady state within ~ 3 ms after the ELM event. In the other discharge, the pressure gradient just inboard of the last closed flux surface reached a steady state early in the ELM recovery phase even as the pedestal expanded into the core and the maximum pressure gradient continued to rise during the remainder of the ELM cycle. Simple quantitative theoretical metrics show that pressure gradients in both discharges reached levels that were large enough to excite kinetic ballooning modes. In addition, the peeling-ballooning theory for the onset of Type-I ELMs and the EPED1 model for pedestal height and width make predictions consistent with the data of both discharges.

1. INTRODUCTION

Obtaining a predictive model for the height of the H-mode pedestal is an important topic of contemporary tokamak research. This research is strongly driven by a need to provide good predictions of pedestal height in future machines, such as ITER [1], due to experimental [2–4] and theoretical evidence [5,6] that global plasma performance increases as the height (pressure) of the H-mode pedestal increases. There are several other important issues of pedestal physics for contemporary and future machines, including control of edge localized modes (ELMs), particle control, shielding of impurities, fuelling and the density limit. In this paper, attention is focused on the physics that controls the pedestal structure and therefore the pedestal height.

A recently developed model, called EPED1 [7], is a physics-based model that has provided good predictions of pedestal height and width in DIII-D and other devices [7–9]. This model is based on a combination of two hypotheses from MHD theory. The first hypothesis is that the maximum achievable pedestal pressure is limited by the onset of finite- n ideal peeling-ballooning MHD modes [10,11]. Linear versions of this theory have been embodied in numerical codes and used to compute whether experimental pedestal pressure and current density profiles are stable to these modes. The linear theory has successfully described the limits to achievable pressure profiles as measured in a number of tokamaks and a wide variety of plasma conditions [12]. The Type I ELM instability is now understood as an MHD stability that is triggered when edge pressure and current densities reach the threshold for destabilization of peeling-ballooning modes. A predictive capability for the energy and particle transport caused by these modes requires the development of non-linear theory, an area of active research.

The second hypothesis of the EPED1 model is that the pedestal pressure gradient triggers kinetic ballooning modes even before the pedestal reaches the peeling-ballooning limit [7]. When these modes are active, they are predicted to strongly limit the achievable pressure gradient and to help set the width of the pedestal. The theory predicts that the resulting pedestal width Δ is approximately equal to $0.1(\beta_{\theta,ped})^{1/2}$ where $\beta_{\theta,ped}$ is the beta-poloidal measured at the top of the pedestal. As used in the theory, Δ is the average of the widths of the electron density and electron temperature widths and is measured in units of normalized poloidal flux and $\beta_{\theta,ped}$ is obtained from twice the electron pressure at the top of the pedestal. The pedestal parameters are obtained from standard fits of a tanh function to pedestal profiles. Experimental data from a wide range of discharges in DIII-D have been used to obtain an empirical value of the coefficient in the width scaling with the result being $\Delta = 0.076(\beta_{\theta,ped})^{1/2}$. This expression for width is used in the EPED1 model.

An experiment was performed in DIII-D to test the EPED1 model against experimental data. The EPED1 model successfully described the experimentally achieved values of the pedestal pressure height, which was varied by more than an order of magnitude, and the pedestal width, which was varied by a factor of three [7,8]. The measured widths exhibited the predicted $(\beta_{\theta,ped})^{1/2}$ dependence. Similar scalings have been found on other machines. Initial tests in C-Mod show a width scaling consistent with $(\beta_{\theta,ped})^{1/2}$ [9]. Widths of the electron temperature profile in AUG are consistent with a $(\beta_{\theta,ped})^{1/2}$ scaling, but other powers of $\beta_{\theta,ped}$ cannot be ruled out [13]. All of these measurements are for widths obtained just before an ELM. However, data from some discharges in DIII-D have also exhibited this width scaling during the pedestal evolution between ELMs [8,14].

These results show that the EPED1 model has had significant success in describing pedestal structure in several experiments. This success motivates further experimental studies of the model, particularly studies to test the hypothesis that kinetic ballooning modes limit the pedestal pressure gradient. If this hypothesis is true, it is expected that the modes would be excited when the maximum pressure gradient reaches a threshold value to trigger the modes. If transport from the modes were sufficiently strong, the onset of the modes would locally provide a strong constraint on the pressure gradient. Thus, a clamping of the maximum pressure gradient or a marked reduction in the rate of rise of the pressure gradient could be signatures of the modes. The purpose of this paper is to look for these signatures in data from DIII-D discharges. The approach taken is to examine the temporal evolution of the total pressure and its gradient during the ELM cycle of two DIII-D discharges. A second purpose of this paper is to examine the predictions of peeling-ballooning theory and of the EPED1 model for these discharges.

The structure of this paper is as follows. Section 1 provides an overview and introduction. Section 2 discusses experimental measurements of the temporal evolution of the pressure profiles during the ELM cycle of two different discharges. One discharge was developed to emulate the ITER baseline scenario; the other discharge was operated at high beta-poloidal. Section 3 discusses the observed pressure gradients in terms of predictions from the peeling-ballooning theory and expected signatures for kinetic ballooning modes. An MHD code that computes the onset conditions for infinite-n ideal ballooning modes is used to predict simple quantitative metrics for the onset of kinetic ballooning modes. A summary and conclusions are presented in Section 4.

2. EXPERIMENTAL MEASUREMENTS OF PEDESTAL PRESSURE PROFILE EVOLUTION

The evolution of edge profiles and their gradients through an average ELM cycle is examined in detail for two DIII-D discharges. These profiles include the electron density, electron temperature, ion temperature and total plasma pressure. The discharges in this experiment were produced with a long steady state phase during which Type I ELMs limited the pedestal pressure. All auxiliary heating was via injection of deuterium neutral beams; the fuelling gas was deuterium for all discharges discussed.

Pedestal profiles were obtained during phases of these discharges when global plasma parameters, such as line averaged density and beta, were approximately in steady state, in a way that has been described elsewhere [14,15]. Briefly, this analysis starts with the determination of ELM timing in a discharge from a divertor D_α signal. The period between each pair of adjacent ELMs is typically sub-divided into five intervals to represent time during the recovery of the pedestal during the inter-ELM cycle. For each of the selected intervals, profile data are accumulated from appropriate periods between pairs of ELMs during the steady state phase of the discharge. These profile data are fit with analytic functions of the flux coordinate ψ_N , as discussed elsewhere [15]. Fits of the electron density n_e and electron temperature T_e include a tanh function to model the pedestal; fits of the ion temperature usually use a spline function to model the pedestal.

The total pressure p_{TOT} is obtained as the sum of the electron pressure, the main ion pressure, the carbon pressure and the fast ion pressure. A Thomson scattering (TS) system [16] is used to measure n_e and T_e . A charge exchange recombination [17] system is used to measure the ion temperature T_i and the density of fully ionized carbon. Since carbon is the dominant low-Z impurity, the main ion density is obtained from measurements of the electron and carbon densities. Magnetic equilibrium reconstructions used in the fitting procedures are obtained from the EFIT code [18]. These equilibria are computed for the time of each Thomson scattering laser pulse and are based on standard magnetic measurements. Finite current density is allowed at the separatrix to emulate the pedestal bootstrap current. (More accurate calculations of current density are performed for kinetic equilibria, used in MHD stability calculations, as discussed later.) The fast ion pressure is computed from the ONETWO 1.5D transport code [19], which uses a Monte Carlo algorithm (NFREYA) to compute the fast ion birth profile and an analytic treatment to compute the slowing down of the fast ions [20]. The computed fast ion pressure in

the pedestal is negligible compared to the pedestal thermal pressure. The fast ion pressure is included here primarily for purposes of calculating kinetic equilibria, required for MHD stability calculations, as will be discussed later. The fast ion pressure can be 20%–30% of the core pressure in some discharges, and it is necessary to account for this pressure to attain the best possible accuracy in kinetic equilibria.

2.1. Pedestal Evolution In ITER Demonstration Discharge

Discharges developed to study the ITER baseline scenario [21] have long periods between ELMs and exhibit a large variation of pedestal parameters during the inter-ELM cycle. Due to these factors, these discharges provide clear trends on the evolution of pedestal profiles between ELMs. Figure 1 shows waveforms for one of these discharges (#131498) over the time of interest, which is 3150–4650 ms. These waveforms include the neutral beam injection (NBI) power (with 40 ms smoothing), the line-averaged density, the volume-averaged poloidal beta β_θ , the stored magnetic energy W_{dia} obtained from a fast diamagnetic loop, the electron pressure at the top of the pedestal $p_{e,ped}$, the pedestal electron density $n_{e,ped}$, the pedestal electron temperature $T_{e,ped}$, the pedestal ion temperature $T_{i,ped}$ and a divertor D_α signal, which shows spikes due to ELM instabilities. The pedestal electron parameters are obtained from tanh analysis of individual TS pulses [22] and $T_{i,ped}$ is obtained from a single chord charge exchange recombination (CER) measurement with a spatial view of normalized poloidal flux $\psi_N = 0.88$ – 0.95 during the time of interest. During the time of interest, this discharge had large, quasi-periodic ELMs, as can be easily seen in the D_α , W_{dia} and $p_{e,ped}$ traces. In addition, $p_{e,ped}$ increased by a factor of ~ 4 – 5 between ELMs, which had an average period of about 180 ms in this discharge. The global β_θ was nearly constant during the time of interest, whereas the line-averaged density increased by $\sim 20\%$ – 30% during the time of interest because the discharge shape was not optimized for pumping and density control. All pedestal parameters show drops at ELM events with subsequent recoveries. The maximum values of these parameters achieved between ELMs remained approximately constant. There is a significant outlier point in all the electron pedestal parameters at about 3950 ms, a time when the TS laser fired during an ELM event. The $T_{i,ped}$ waveform has some gaps due to modulation of the neutral beam used to make this measurement.

Taken together, the divertor D_α and W_{dia} signals in Figure 1 are useful to judge the degree to which ELMs were alike. The D_α trace shows that the ELMs exhibited an approximately periodic character with the biggest deviation being the relatively long period between ELMs from ~ 4200 – 4400 ms. This trace shows no evidence of a complex or compound ELM structure due to

interspersing of larger and smaller ELMs. The drops in the W_{dia} signal at each ELM crash are a measure of the size of the ELM events. This signal shows that there was not a large variation (more than a factor of \sim two) in ELM size and that the average ELM size remained about constant through the time of interest. Clearly, though, the ELM cycles were not identical and it cannot be expected that the pedestal profiles of temperature and density were identical for various phases of the different ELM cycles. Thus, variability of ELM sizes and inter-ELM periods is a systematic issue that may affect the analysis procedure used here.

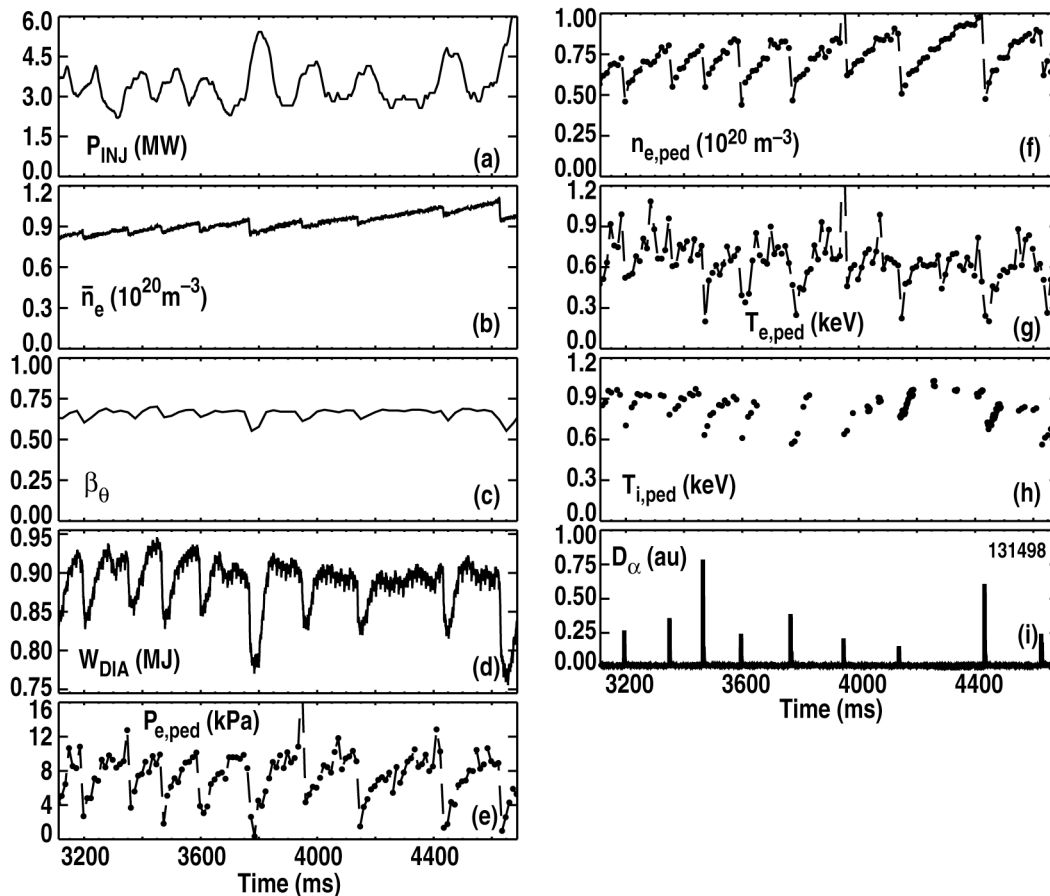


Figure 1. Waveforms from discharge 131498, an ITER baseline demonstration discharge: (a) injected beam power, smoothed with a 40 ms boxcar filter, (b) line-averaged electron density, (c) global beta-poloidal, (d) diamagnetic stored energy, (e) pedestal electron pressure, (f) pedestal electron density, (g) pedestal electron temperature, (h) pedestal ion temperature, (i) divertor D_{α} signal. Time of interest is 3150–4650 ms.

Pedestal profile measurements have been accumulated over the multiple ELMs in the time of interest and have been used to construct the temporal evolution of profiles for an “average” ELM cycle. As used here, the term “ELM cycle” means “inter-ELM cycle”, the period from the end of one ELM to the onset of the next ELM. Profiles have been generated for various portions of the

average ELM cycle, including the 5%–20%, 20%–40%, 40%–60%, 60%–80% and 80%–99% phases. The 5%–20% phase is early in the recovery of the pedestal from an ELM crash and the 80%–99% phase is just before an ELM crash.

The temporal evolution of profiles of n_e , T_e , T_i , electron pressure p_e , ion pressure p_i and p_{TOT} are shown in Figure 2. All profiles show continuous increases through all phases of the ELM cycle. It can be seen in both the plot of total pressure in Figure 2(f) and in the plot of $p_{e,ped}$ in Figure 1 that the rate of rise of the pressure decreased during the ELM cycle. However, these two plots provide a different quantitative assessment of the increase of pedestal pressure during the ELM cycle. Figure 2(f) shows that the p_{TOT} profile increased by a factor of ~ 2 from early to late in the ELM cycle. In contrast, the $p_{e,ped}$ trace of Figure 1, which is obtained without averaging over any time bin, show that the electron pedestal pressure varied by a factor of ~ 4 during a typical ELM cycle. The picture provided by these data is that there is an initial rapid recovery of the pedestal from an ELM crash and that profiles averaged over the initial $\sim 20\%$ of the ELM cycle average over some of this evolution.

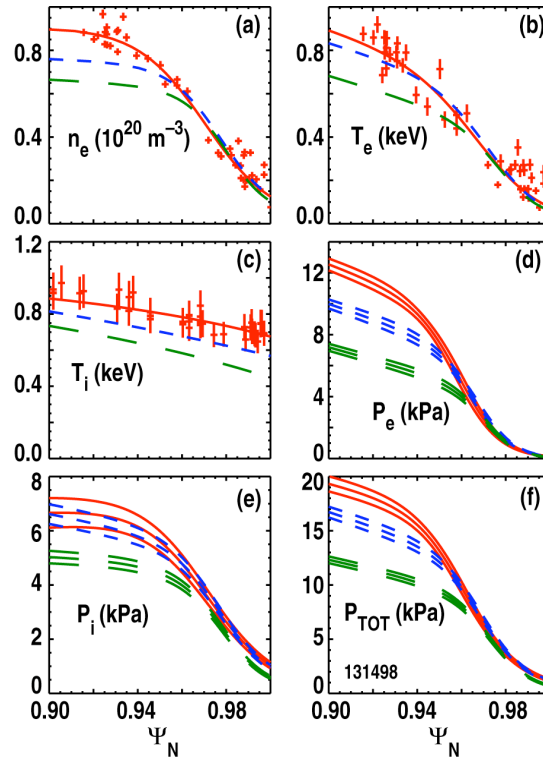


Figure 2. Pedestal profiles for discharge 131498: (a) electron density, (b) electron temperature, (c) ion temperature, (d) electron pressure, (e) ion pressure and (f) total pressure. In each panel, fits to experimental profiles are shown for 5%–20% (long dash), 20%–40% (short dash) and 80%–99% (solid line) intervals of the ELM cycle. Experimental data are shown for the 80%–99% interval. Three-sigma error bands are shown for the pressure profiles. Fast ion profile is shown in panel (f) but is indistinguishable from x-axis line.

The gradients of n_e , T_e , T_i , p_e , p_i and p_{TOT} also show a clear evolution throughout the ELM cycle of discharge 131498, as shown by Figure 3. The gradient of p_{TOT} achieved a steady state profile for $\psi_N > 0.98$ by the 5%–20% interval of the ELM cycle. The gradient in this region remained very nearly constant during the subsequent ELM evolution as the radial extent of the high gradient region grew inwards to smaller values of ψ_N . As a consequence, the peak value of the pressure gradient increased through the ELM cycle and its location moved inwards. In addition, the width of the high gradient region increased by $\sim 50\%$ during the ELM cycle during this inward expansion. These changes are partially due to similar changes in the gradients of n_e , T_e . For both quantities, the width of the high gradient region for these quantities increased and the inner edge of the high gradient region expanded inwards throughout the ELM cycle. This behavior can be seen directly in the underlying profiles of n_e and T_e (Figure 2). Figure 3 shows that the width of the steep gradient region for both profiles increased during the ELM cycle. In contrast, the gradient of T_i decreased through the ELM cycle over most of the pedestal region due to rising T_i near the separatrix.

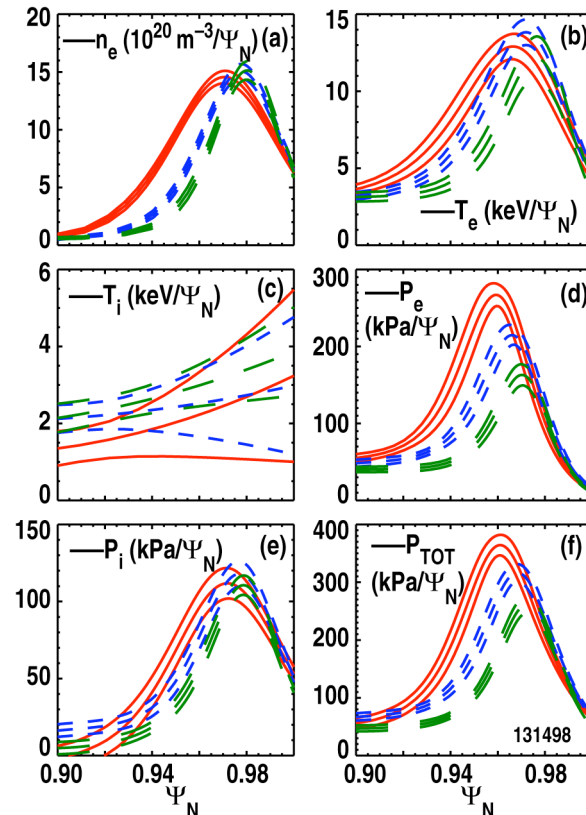


Figure 3. Gradients of fits to pedestal profiles with respect to ψ_N for discharge 131498: (a) gradient of electron density, (b) gradient of electron temperature, (c) gradient of ion temperature, (d) gradient of electron pressure, (e) gradient of ion pressure and (f) gradient of total pressure. In each panel, gradients are shown for 5%–20% (long dash), 20%–40% (short dash) and 80%–99% (solid line) of the ELM cycle. Three-sigma error bands are shown for the all profiles.

These observations on evolution of profiles and their gradients are made with regard to error bars on the measured data points for n_e , T_e and T_i in Figure 2, plus error bands shown on the pressure profiles in Figure 2 and their gradients, shown in Figure 3. A Monte Carlo process has been used to compute the error bands, based on the error bars of the measurements. No account was taken of uncertainties in the fast ion pressure or density, due to very small values in the pedestal. In this process, one hundred estimates of the density, temperature and pressure profiles were computed by the same process. For each different computation of these profiles, all input measurements were varied randomly within their error bars. Thus, at each spatial point for which an unperturbed profile was evaluated, the one hundred perturbed profiles were used to compute a standard deviation about the original unperturbed profile. These standard deviations are an estimate of the random error in the underlying profiles. Due to the large number of data points, the computed standard deviations are generally quite small. In order to provide a conservative approach to examining the effect of these errors on the evolution of profiles, the error bands shown in Figure 2 are taken as ± 3 times the standard deviation. Error bands on gradients were generated in the same way. For a given unperturbed profile, gradients were computed for each of its one hundred perturbed profiles. The error bands shown in Figure 3 are ± 3 times the standard deviations of the perturbed gradients, as computed in this way.

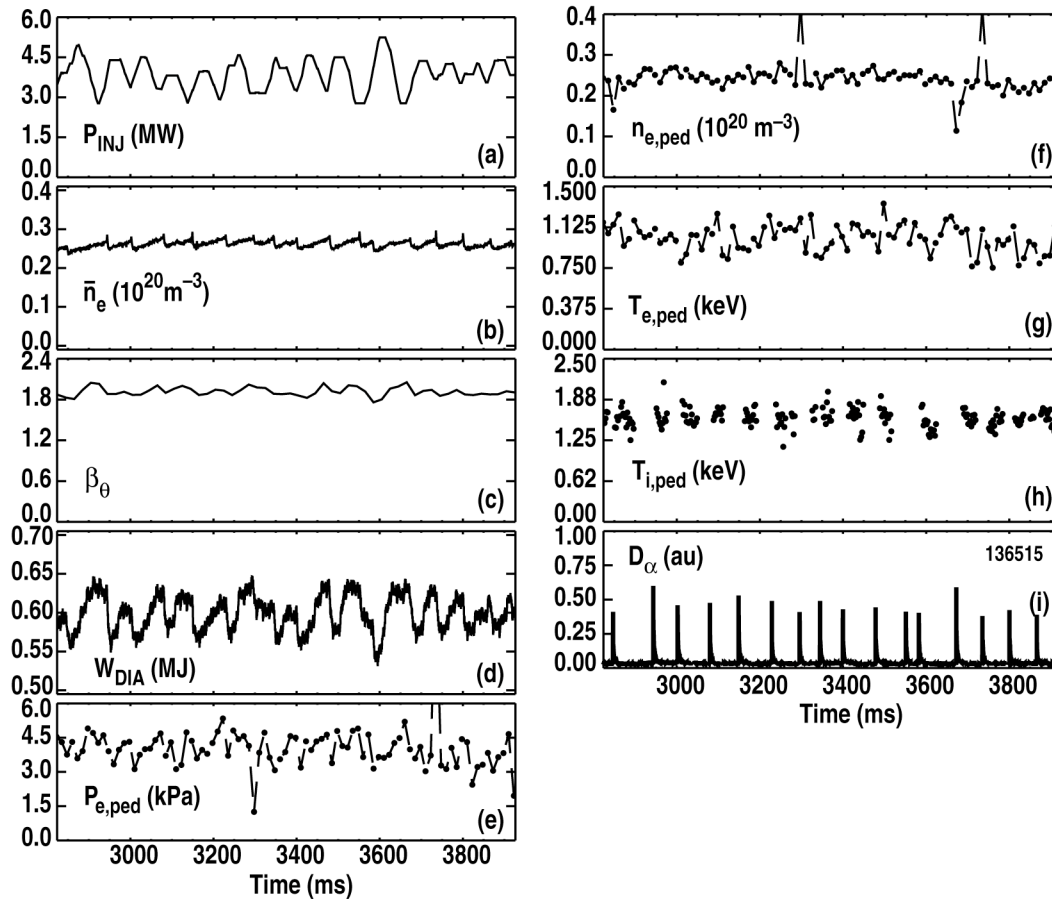


Figure 4. Waveforms from discharge 136515 at low I_p (0.71 MA) and high global β_p (1.9): (a) injected beam power, smoothed with a 25 ms boxcar filter, (b) line-averaged electron density, (c) global beta-poloidal, (d) diamagnetic stored energy, (e) pedestal electron pressure, (f) pedestal electron density, (g) pedestal electron temperature, (h) pedestal ion temperature, (i) divertor D_α signal. Time of interest is 2850–3900 ms.

There is potential for systematic errors in the profile analysis. Procedures used in the analysis attempt to minimize some of the major known sources of systematic error. One obvious systematic problem is that individual ELM cycles are not identical. To minimize this source of error, it is important to select phases of discharges which have relatively periodic ELMs, although this can never be perfectly achieved. However, the process of generating composite profiles from many individual profile measurements has been adopted in order to reduce scatter in results obtained from analysis of individual profiles. This strategy generally works well, despite the fact that ELM cycles are not identical. Another source of systematic error is possible errors in mapping of data from physical coordinates to flux coordinates, due to uncertainties in computing magnetic equilibria. For the analysis discussed here, this source of error is primarily a concern for the alignment of the n_e and T_e profiles relative to the separatrix. In order to accommodate this concern, the mapping of the n_e and T_e is adjusted by a small amount so that

T_e at the separatrix is consistent with values expected from parallel electron thermal conduction on the open field lines. The procedure is discussed in detail elsewhere [14,15]. Another possible systematic error arises from the fact that the main ion density is not measured directly but must be inferred from measurements of carbon densities and electron densities. For typical moderate concentrations of carbon, this source of error is not expected to be large. Another source of error comes from the particular fitting functions that are used. These functions impose some structure on the results and could particularly affect computations of gradients. This is an unavoidable issue because there is no physics basis for choosing a specific fitting function. The approach used is to fit the data as reliably as possible. The success of this approach can be judged from the fit lines to data. One of the main goals of the work discussed here is to examine trends of profiles and their gradients. For this purpose, it is expected that possible systematic errors will roughly affect all profiles in the same way and will not qualitatively affect relative changes between the profiles.

2.2. Pedestal Evolution In High Beta-Poloidal Discharge

Another experiment was performed on DIII-D to study the temporal evolution of the pedestal pressure and its gradient. A significant goal of the experiment was to produce a discharge with a high pedestal beta poloidal $\beta_{\theta,ped}$, which was expected to have a wide pedestal and therefore to allow for good spatially resolved measurements of pedestal structure. This width prediction is obtained from the pedestal width scaling in the EPED1 model. The discharges in this experiment were all obtained with neutral beam heating, were in the Type-I ELMing regime and were produced with a lower single null configuration with the grad-B drift towards the X-point. Cryopumping was used to help control the plasma density. Some of the main discharge parameters for this experiment were toroidal magnetic field $B_T = 2.14$ T, $I_p = 0.71$ MA, normalized toroidal beta $\beta_N \sim 2.2$ (obtained by feedback on the neutral beam injection power), global beta-poloidal β_θ of 1.9, upper triangularity $\delta_{up} \sim 0.38$ and lower triangularity $\delta_{low} \sim 0.70$.

Several repeat discharges were obtained with these parameters and Figure 4 shows waveforms for one of these discharges (#136515) over the time of data accumulation, which was from 2850 to 3900 ms. These waveforms have the same meaning as in Figure 1, except that $T_{i,ped}$ was obtained from a tanhfit to data from the CER system. The density and β_θ waveforms show some modulation due to ELMs but are constant in a time-averaged sense over the time interval of interest. The D_α trace shows that the ELMs exhibited an approximately periodic character with the biggest deviation being the two closely spaced ELMs just before 3600 ms. This trace shows no evidence of a complex or compound ELM structure due to interspersing of larger and smaller

ELMs. The drops in the W_{dia} signal show that there was not a large variation (more than a factor of \sim two) in ELM size and that the average ELM size remained about constant through the time of interest. The pedestal values for p_e , n_e , T_e and T_i , obtained from tanhfits to single profiles, show relatively little variation during this time and show much smaller effects than seen for the ITER demonstration discharge. The maximum pedestal electron pressure between ELMs remained approximately constant; the two main outlier points for this pressure are from times when the TS laser fired during an ELM event.

Composite profiles, obtained for an average ELM cycle during the time of interest, show relatively little evolution during the ELM cycle. Figure 5 shows that pedestal profiles for n_e , T_e , p_e , p_i and p_{TOT} increased by small amounts from the 20%–40% to the 80%–99% intervals of the ELM cycle. The T_i profiles for these two intervals are nearly identical. The gradients of these profiles, shown in Figure 6, show similar behavior. There are small increases in most gradients; there is no clear evidence of a broadening of the high pressure regions, as was seen for the ITER demonstration discharge. As shown by the W_{dia} trace in Figure 4, the ELMs were large, with about 10%–15% of the plasma energy lost at an ELM. The profile evolution data imply that the pedestal in these high β_θ discharge recovered quickly after an ELM crash, with most recovery occurring within the first 0%–20% of the ELM cycle. The maximum gradients did not change markedly during the remaining portion of the inter-ELM period.

The temporal evolution of pedestal parameters of this discharge have been studied with higher time resolution by using repeat discharges to provide additional data for constructing composite profiles. The procedure for assembling data uses multiple ELMs from the same time of interest for these discharges. The data have been accumulated from nine repeat discharges and sorted into bins of 3 ms duration, with the first bin starting at the onset of an ELM crash. Fitting was performed with the standard five-parameter tanhfit function [22]. Figure 7 shows pedestal heights and pedestal gradients for n_e , T_e , T_i and p_e as computed with this procedure for an effective ELM cycle. These data show that by 3–6 ms after the ELM crash, the pedestal heights and gradients had reached nearly their maximum values and did not evolve significantly through the remainder of the ELM cycle. The one exception might be the electron pedestal density, which shows a slight increase from the beginning to the end of the ELM cycle. Thus, for these high β_θ discharges, the temporal buildup of the pedestal gradients after the ELM crash is unresolved. Whatever mechanism limited the gradients was operative very early in the ELM cycle.

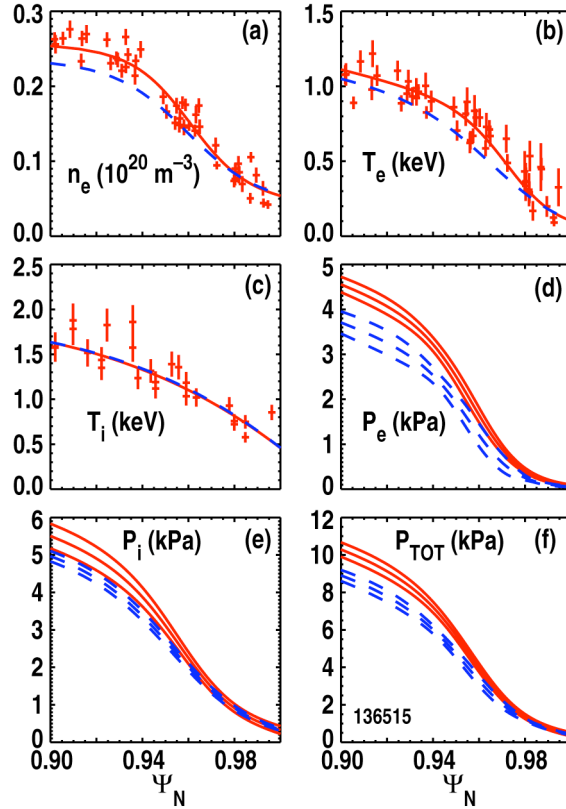


Figure 5. Pedestal profiles for discharge 136515: (a) electron density, (b) electron temperature, (c) ion temperature, (d) electron pressure, (e) ion pressure and (f) total pressure. In each panel, fits to experimental profiles are shown for 20%–40% (short dash) and 80%–99% (solid line) intervals of the ELM cycle. Experimental data are shown for the 80%–99% interval. Three-sigma error bands are shown for the pressure profiles. Fast ion profile is shown in panel (f) but is indistinguishable from x-axis line.

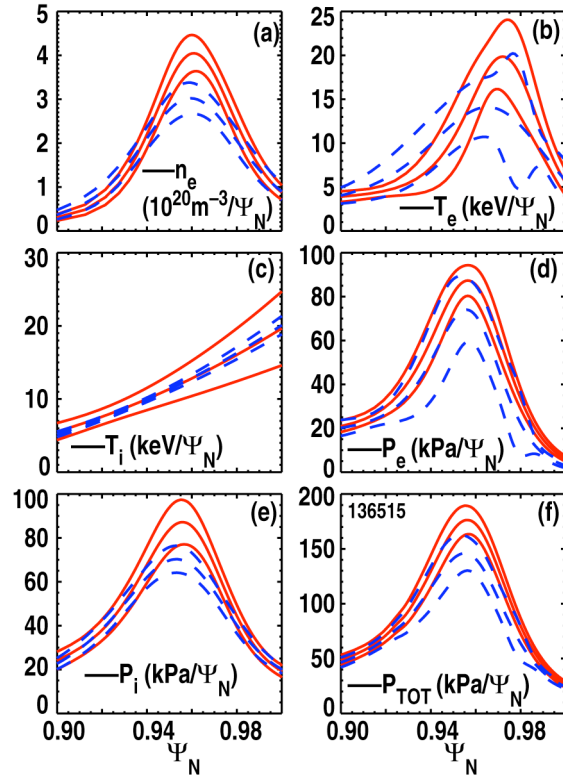


Figure 6. Gradients of fits to pedestal profiles with respect to ψ_N for discharge 136515: (a) gradient of electron density, (b) gradient of electron temperature, (c) gradient of ion temperature, (d) gradient of electron pressure, (e) gradient of ion pressure and (f) gradient of total pressure. In each panel, gradients are shown for 20%–40% (short dash) and 80%–99% (solid line) of the ELM cycle. Three-sigma error bands are shown for the all profiles.

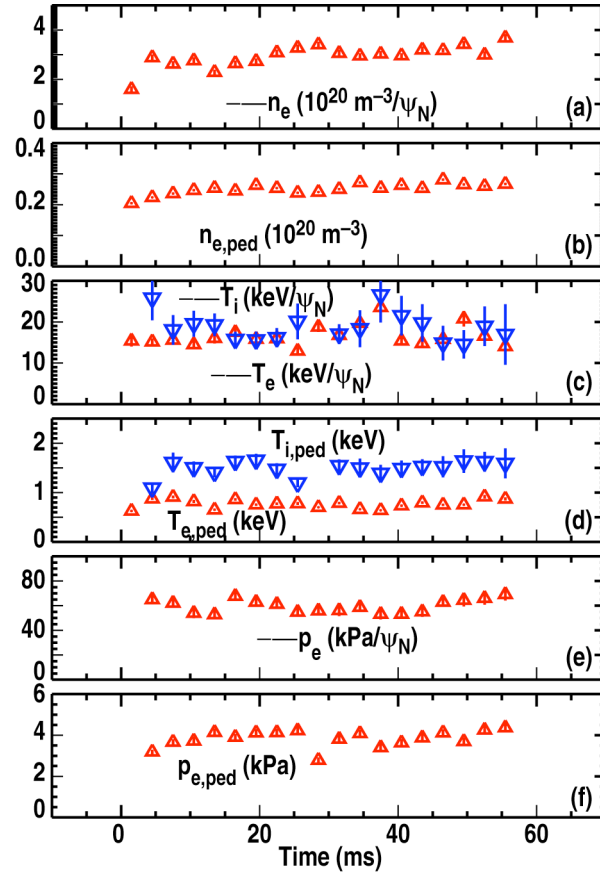


Figure 7. Time evolution of pedestal parameters obtained from composite ELM cycles from 9 repeat discharges. Time is relative to ELM crash. (a) Maximum gradient of electron density pedestal, (b) height of electron density pedestal, (c) maximum gradient of electron temperature pedestal (triangles) and ion temperature pedestal (triangles pointing down), (d) height of electron temperature pedestal (triangles) and ion temperature pedestal (triangles pointing down), (e) maximum gradient of electron pressure pedestal and f) height of electron pressure pedestal.

As part of the experiment to obtain data for the high β_θ discharges, data were also obtained at other currents and densities. Profile analysis has also been performed for two of these discharges, which were both operated at 1.3 MA. The discharges differed in density. One discharge operated near the lowest attainable density; the line-averaged density of the second discharge was increased by $\sim 25\%$ – 30% with heavy gas puffing. The analysis of these discharges provides similar results to those obtained for the 0.7 MA, high β_θ discharges. Pedestal gradients observed in the 20%–40% intervals of the ELM cycles were close to the values obtained in the 80%–99% intervals.

3. COMPARISON OF EXPERIMENTAL PRESSURE PROFILES TO THEORY

The data discussed in Section 2 will be compared to predictions from both the theory of finite- n ideal peeling-ballooning modes and from predictions that kinetic ballooning modes limit the pressure gradient during buildup of the pedestal.

3.1 Limits to Pedestal Pressure as Predicted by Peeling-Ballooning Theory

One of the hypotheses of the EPED1 model is that finite- n ideal peeling ballooning modes place stringent limits on the attainable pedestal pressure. There are codes available that can be used to compute the linear stability threshold of these modes in the pedestal. One of these codes, ELITE [10,11], has been used to examine the stability of the discharges discussed in the previous section. In the theory of peeling-ballooning modes, the edge current density and pressure gradient are the parameters that control stability. Therefore, a pre-requisite for running ELITE is the availability of an MHD equilibrium that has the most accurate possible representation of the edge current density and pressure gradient. The equilibria used here have been obtained from a “kinetic” equilibrium reconstruction with the EFIT code. In addition to the usual magnetic diagnostics, this reconstruction uses the measured total pressure profile to help constrain the equilibrium fit, measurements from a motional Stark effect diagnostic [23] to constrain the internal current density and calculations of the neoclassical bootstrap current from the Sauter model [24,25] to constrain the current in the pedestal.

The stability properties to peeling-ballooning modes of the ITER demonstration discharge 131498 are examined in Figure 8. The solid curve is the stability threshold computed with the ELITE code for the 80%–99% interval of the ELM cycle. This curve is parameterized in terms of normalized edge current density and normalized pressure gradient [12]. Stability thresholds have been computed for other sub-intervals of the ELM cycle and these are all very similar to the threshold for the 80%–99% interval. The other sub-intervals include the 0%–10%, 5%–20%, 10%–30%, 20%–40%, 40%–60% and 60%–80% intervals. The operating points for these sub-intervals from the experiment are shown in Figure 8. These data show that the operating point for the 0%–10% interval, which corresponds to the beginning of the ELM cycle, lay deep in the predicted stable part of the operating space. The data also show that as the ELM cycle progressed in time, the operating points monotonically approached the predicted threshold for the onset of the ELM instability. The operating point for the 80%–99% interval was at the threshold for ELM

instability within experimental uncertainty. This figure demonstrates that the peeling ballooning model successfully predicts the allowable operating space for the pedestal of discharge 131498.

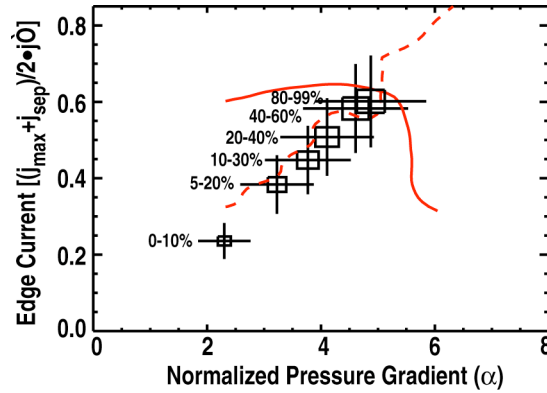


Figure 8. Solid line is computed threshold for onset of ELM stability for discharge 131498 in a space of normalized pedestal current density and normalized pedestal pressure gradient, with stable operating space being below the line. Line is computed with ELITE code and established from the criterion $\gamma = \omega_{*pi}/2$. Data points are experimental values obtained at different intervals of the ELM cycle. Interval of the ELM cycle for each data point is noted to the left of the point. Data point for 60%–80% nearly coincides with data point for 40%–60% and is not shown. Dashed line shows predicted trajectory for KBM stability, based on predictions from BALOO code.

Peeling-ballooning stability of the high β_θ discharge 136515 is examined in Figure 9, which shows the pedestal operating space in terms of normalized current density and normalized pressure gradient. The stability boundaries were computed from the kinetic equilibrium obtained from the 80%–99% interval of the ELM cycle for this discharge. The solid line shows the computed threshold for instability, obtained from the criterion $\gamma = \omega_{*pi}/2$, where ω_{*pi} is the ion diamagnetic drift frequency and γ is the linear growth rate for the fastest growing peeling-ballooning mode. Dotted lines show contours of growth rate for $\gamma = 0.5(\omega_{*pi}/2)$ and $\gamma = 1.5(\omega_{*pi}/2)$. The experimental operating point for the 80%–99% interval of the ELM cycle is also shown and was at the computed instability threshold within experimental uncertainties. Thus, peeling-ballooning theory predicts the limits to the operating space for the pedestal of this discharge.

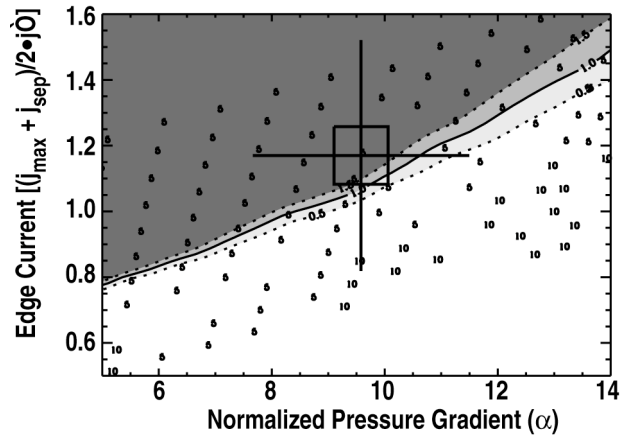


Figure 9. Solid line is computed threshold for onset of ELM stability for discharge 136515 in a space of normalized pedestal current density and normalized pedestal pressure gradient, with stable operating space being below the line. Line is computed with ELITE code and established from the criterion $\gamma = \omega * \pi / 2$. Dotted lines are drawn for $\gamma = 0.5(\omega * \pi / 2)$ and $\gamma = 1.5(\omega * \pi / 2)$. Experimental data point is from the 80%–99% interval of ELM cycle. Numbers in background of plot are n numbers of most unstable modes. Mode numbers checked are multiples of 5 (5, 10, 15, ...).

3.2. Examination Of Pressure Gradient In Terms Of Kinetic Ballooning Theory

As noted earlier, kinetic ballooning modes are predicted to turn on quickly and to manifest themselves by significantly reducing the time rate of increase of the maximum pedestal pressure gradient. This is a qualitative prediction without a quantitative prediction of what pressure gradient would be needed to drive the modes. One way to look for signatures of this behavior is to examine the evolution of the pressure gradients for the various discharges through the ELM cycle, as has been discussed in Section 2. For discharge 136515, the pressure gradient had little evolution during the ELM cycle. This is most clearly demonstrated in Figure 7, which shows that within a few ms after an ELM crash, the electron pressure gradient was saturated or nearly saturated and had little evolution for most of a 50–60 ms ELM cycle. The available measurements are not fast enough to show the evolution of the gradient in the early part of the ELM cycle. Clearly, some physics provided strong limits to the gradient very early in this ELM cycle. Kinetic ballooning modes are a candidate for this physics.

In the ITER demonstration discharge, the maximum pressure gradient increased throughout the ELM cycle, with the rate of rise decreasing as the ELM cycle progressed. Already in the 20%–40% interval, the pressure achieved about 85% of its ultimate value, as shown in Figure 3(f). There is no signature that some mechanism turned on during the ELM cycle to halt the increase of the maximum gradient. However, as was noted in the discussion of Figure 3(f), the pressure gradient in the outer regions of the pedestal achieved equilibrium very early in the ELM

cycle. Thus, if pressure gradient limiting phenomena were operative, they may have acted first near the separatrix in this discharge.

Kinetic ballooning modes (KBM) are predicted to have very similar onset conditions as ideal infinite- n ballooning modes in the absence of second stability [26–29]. Therefore, knowledge of threshold conditions for these high- n modes is applied here to the study of kinetic ballooning modes. It should be noted, though, that the link between infinite- n ballooning modes and KBMs has been established primarily for conditions of the plasma core with relatively few studies done for edge conditions. Thus more work is needed to determine what limits apply to the use of infinite- n theory for the study of KBMs in pedestal conditions. The effect of edge geometry on kinetic ballooning physics is one such issue that needs further study. With this caveat, the BALOO code [30], developed to study infinite- n ballooning modes in non-circular tokamak geometry, has been used to make predictions for the onset conditions of kinetic ballooning modes in the pedestal. Insights gained with analysis of many DIII-D discharges with BALOO show that the pedestal typically is in a parameter space where the critical value of α for driving infinite- n ballooning modes scales as $\alpha \sim 1/s^{1/2}$ with α being the normalized pressure gradient and s the local magnetic shear on the outboard side of the plasma [7]. Therefore, the pressure gradient for the onset of KBMs is also expected to show an $\alpha \sim 1/s^{1/2}$ scaling.

Calculations with BALOO have been used to make a further quantification of this scaling. These studies have developed the approximate metric that KBMs will be unstable for $\alpha s^{1/2} > 6$, with the metric not valid if the shear is too close to zero or negative. The values of s and α obtained in the discharges discussed here are most likely to meet this criterion for KBM onset in the outer half of the pedestal. Figure 10 shows an example of profiles of α and of $\langle s \rangle$, the flux-surface value of the magnetic shear [31] in the pedestal, for the 20%–40% interval of discharge 136515. These profiles have been obtained from a kinetic equilibrium reconstruction with the EFIT code. The use of a kinetic equilibrium is important, because it provides the best available values for the edge current density and therefore the magnetic shear. As noted previously, these reconstructions use measurements from an MSE diagnostic to constrain the internal current density and calculations of the neoclassical bootstrap current to constrain the current in the pedestal. These computations assume that the edge current density has evolved to the full level expected from the bootstrap current. It should also be noted that the local magnetic shear at the outboard midplane is lower than the flux surface averaged shear. With these caveats and with $\langle s \rangle$ as a proxy for s , the data of Figure 10 imply that the metric for onset of kinetic ballooning modes would be met in the outer part of the pedestal, for ψ_N greater than ~ 0.96 . More experimental and theoretical work is required to provide a more precise estimate of the threshold conditions for

these modes. However, these initial studies provide evidence that the modes could be present in the pedestal and motivate further pursuit of this subject.

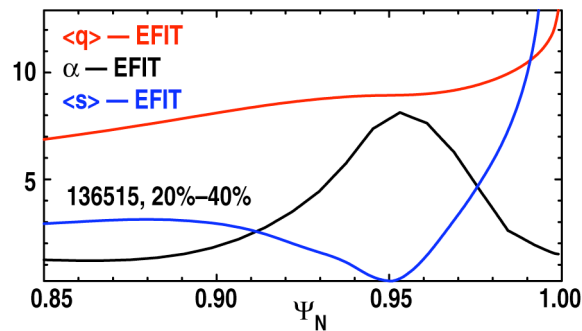


Figure 10. (Color online) Profiles of normalized pressure gradient α (solid line) and flux-surface averaged magnetic shear $\langle s \rangle$ (dashed line) for discharge 136515 during 20%–40% interval of ELM cycle.

A further estimate of the KBM threshold has been made with the BALOO code for the temporal evolution of the maximum pedestal pressure gradient of the ITER demonstration discharge. The code has been used to evaluate a simple prescription for the onset of KBMs. This calculation used the s and α profiles, obtained from kinetic equilibrium reconstructions, for each of the sub-intervals of the ELM cycle, shown in Figure 8. The BALOO code has been used to compute the threshold pressure gradient for which 1% of the pedestal in normalized poloidal flux is unstable to high- n ideal ballooning modes. This threshold is shown as the dashed line in Figure 8. In theory, the plasma is unstable to ballooning modes to the right of the dashed line and stable to the left. Since KBMs have a very similar threshold to high- n ballooning modes, this dashed line is interpreted as a trajectory where the pedestal may have hit a local KBM limit. During the ELM cycle, the experimental operating points followed this trajectory closely, as would be expected if kinetic ballooning modes locally limited the gradient. Certainly this calculation is not a proof that KBMs actually performed this function. Much more work is needed to prove or disprove that hypothesis. But, the results are suggestive and motivate more study of KBMs in the pedestal.

3.3. Predictions From EPED1 Model

One of the hypotheses of the EPED1 pedestal model is that kinetic ballooning modes limit the pressure gradient in the H-mode pedestal. This hypothesis has motivated most of the results discussed in this paper. It is also appropriate to apply the full model to the discharges discussed in this paper.

The EPED1 model has been used to calculate the pedestal pressure height and the pedestal width, with the definitions discussed in Section 1, for the high beta-poloidal discharge and the two related high current discharges (1.3 MA), discussed in Section 2. The predicted heights and widths are compared to the measured heights and widths in Figures 11 and 12 respectively. Also shown are widths and heights from a dedicated experiment performed in 2008 to perform initial tests of the model [7,8] and data from two ITER baseline demonstration discharges (including discharge 131498), also performed in 2008 [7,8]. The EPED1 model predicts the widths and heights of the newer discharges about as well as for the 2008 data except for the data point at the highest predicted pedestal height. This point deviates more than usual from the measured data. This deviation could be due to errors in the evaluation of the experimental data or missing physics in the EPED1 model. One possibility for the latter is that the model uses an approximation to the real geometry in its calculation of stability to peeling-ballooning modes. For the very highly shaped plasmas (high triangularity) used here, the approximation might not be sufficient for best accuracy.

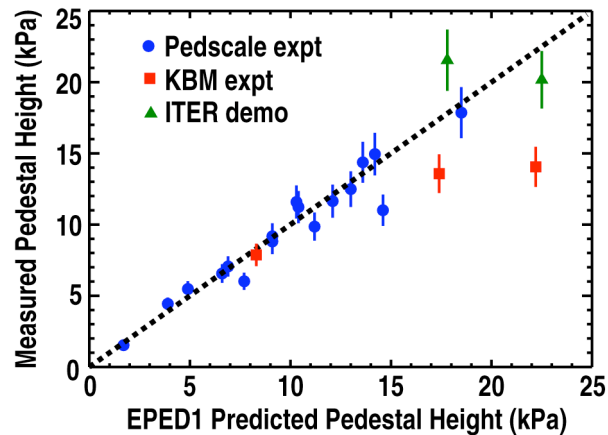


Figure 11. (Color online) Measured pedestal height vs predictions of EPED1 model. Circles are data from first experiment to test the EPED1 model [7,8], triangles are from ITER baseline demonstration discharges [7,8] and squares are from the high triangularity discharges discussed in text. Triangle with lower predicted height corresponds to discharge 131498. Square with lowest height corresponds to discharge 136515.

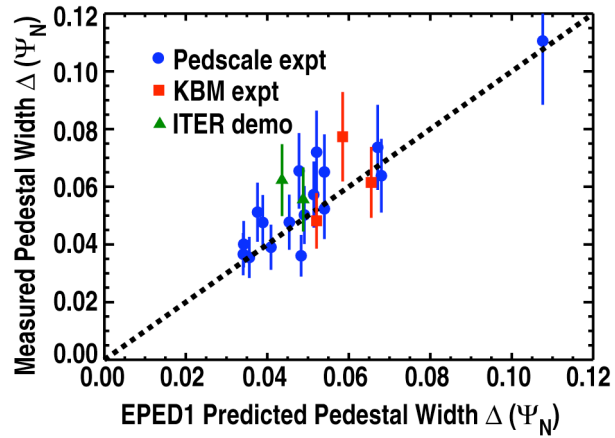


Figure 12. Measured pedestal width vs predictions of EPED1 model. Circles are data from first experiment to test the EPED1 model [7,8] triangles are from ITER baseline demonstration discharges [7,8] and squares are from the high triangularity discharges discussed in text. Triangle with lower predicted width corresponds to discharge 131498. Square with largest predicted width corresponds to discharge 136515.

SUMMARY AND CONCLUSION

The pedestal model embodied in the EPED1 code has provided good quantitative predictions for the pedestal height and width for a range of discharges in DIII-D. This model is a combination of two hypotheses. One hypothesis is that the maximum pedestal pressure is limited by finite- n ideal peeling-ballooning modes. The second hypothesis is that kinetic ballooning modes provide strong constraints on the pedestal pressure gradient even before the ELM instability is reached and that these modes help set the pedestal width, as described elsewhere [7]. The primary goal of this paper is to provide additional tests of the EPED1 model and its two hypotheses. In particular, the pedestal evolution between ELMs has been examined to look for evidence that kinetic ballooning modes play a role in limiting the evolution of the pedestal pressure gradient. Two discharges have been examined in detail. These are an “ITER demonstration” discharge, which had the plasma shape, safety factor and normalized beta of the ITER baseline operation scenario, and a discharge operated at quite high triangularity and global β_θ .

The ITER demonstration discharge, which had a very long ELM period, provided clear data on the evolution of pedestal profiles, including the total pressure and its gradient. This discharge exhibited a rapid recovery from the ELM crash, with the maximum pressure achieving 85% of its final value within the first 20%–40% of the ELM cycle. Nevertheless, the pedestal pressure and maximum pressure gradient continued to increase throughout the ELM cycle with the rate of rise gradually decreasing during the cycle. The maximum pressure gradient continued to evolve due to a broadening of the pedestal width and of the region of large gradients. However, the pedestal pressure gradient did quickly reach saturation in the outermost parts of the pedestal. Thus, the outer portions of the pressure gradient did show behavior that is expected for KBM activity.

Quantitative calculations of peeling-ballooning stability are consistent with the evolution of the pedestal during the ELM cycle for this discharge. Calculations of stability to peeling-ballooning modes show that the operating point of the pedestal was deeply stable early in the ELM cycle. As the ELM cycle evolved, the operating point monotonically moved closer to the threshold for the onset of peeling-ballooning modes and the final operating point was at the predicted ELM threshold within error bars.

Because the threshold conditions for kinetic ballooning modes are expected to be similar to those for infinite- n ballooning modes in the absence of second stability, some quantitative estimates for the threshold of KBMs have been computed with the BALOO code, designed to compute the threshold for infinite- n ballooning modes in noncircular geometry. These estimates have generated the metric that KBMs in typical DIII-D discharges are expected to be unstable for

$\alpha s^{1/2} > 6$, with the metric not being valid for values of shear near zero or negative. This metric is most likely to be met in the outside region of the pedestal, which is the region where the pressure gradient was saturated in this discharge. The BALOO code has been used to compute a threshold pressure gradient for which 1% of the plasma (in terms of normalized poloidal flux) is predicted to be unstable to KBMs. These calculations have produced a trajectory during the ELM cycle that closely follows the evolution of the measured maximum pressure gradient. These calculations are by no means definitive, but they suggest that KBMs (or some other mode) could be locally limiting the pedestal pressure gradient while the inner part of the pedestal continues to evolve.

Similar pedestal phenomenology has been reported previously. Measurements in DIII-D [14] have shown a rapid increase of pedestal gradients during initial recovery from the ELM crash with the rate of rise of the gradients decreasing and even coming to equilibrium during the ELM cycle. A gradual increase during the ELM cycle of the pedestal widths of the electron density and electron pressure profiles has been observed. Fast measurements on ASDEX-Upgrade have also shown rapid recovery of pedestal parameters after an ELM crash [32].

Studies of a high β_θ discharge (plus some repeat discharges) show that the pedestal came to a near equilibrium very early, within ~ 3 ms after the ELM crash. There may have been a small evolution of the profiles, particularly the density and pressure profiles during the remainder of the ELM cycle, but the gradients achieved approximately their maximum values very early in the ELM cycle. This type of behavior could be evidence that KBMs or some other phenomenon turned on early in the ELM cycle and limited the evolution of the pressure gradient. For this discharge, the simple metric for the onset of KBMs, $\alpha s^{1/2} > 6$, was met in the outer part of the pedestal by at least the 20%–40% interval of the ELM cycle or earlier.

Calculations of peeling-ballooning stability are also consistent with the experimental measurements for the 80%–99% interval of the ELM cycle of this discharge. However, with the pressure gradient being near its ultimate limit for much of the ELM cycle (~ 50 ms), there is a question of why it took a long time for an ELM to occur. In the context of the peeling-ballooning theory, this delay is understood as lag of the edge current density relative to the buildup of the pressure gradient. Such a lag might be due to an inductive effect in which the Ohmic current transiently opposes the bootstrap current, which is proportional to the pressure gradient [33]. There is no direct measurement of the current density in this discharge to examine this explanation. However, direct measurements of the recovery of the edge current density have been previously made with a Zeeman polarimetry diagnostic on DIII-D and the results are qualitatively consistent with this explanation. For a Type-I ELMing discharge with an ELM

period of about 100 ms, the measurements show that the buildup of the current density lagged the recovery of the pressure gradient and that the current density was recovering for most of the ELM cycle [34].

The results presented have shown evidence of rapid local saturation of the pedestal pressure gradient, as might be expected from kinetic ballooning modes. Simple quantitative estimates of pressure gradients for which KBMs would be excited are comparable to measured gradients. Thus, further study of the hypothesis that kinetic ballooning modes limit pressure gradients in DIII-D are certainly warranted. Future work will use gyrokinetic codes to compute more precise thresholds for these modes. Fast measurements of the evolution of the pedestal density profile early in the ELM recovery may be very helpful and possibly essential to determine where and how rapidly gradients stop evolving. On DIII-D, a fast profile reflectometer system will be used to look for evidence of gradient-limiting phenomena. Ultimately, a definitive identification of kinetic ballooning modes may require nonlinear gyrokinetic calculations to predict characteristics of fluctuation spectra. Measurements of these predicted fluctuation characteristics correlated to the onset of a limit to measured pedestal gradients would be strong evidence that kinetic ballooning modes play an important role in controlling the pedestal structure.

In summary, measured pressure gradients are of the right magnitude to drive kinetic ballooning modes in the pedestal of H-mode discharges in DIII-D. Some signatures of rapid saturation of gradients have been observed. Much more theoretical and experimental work is required to establish if the modes are really present and if they have a significant effect on pedestal structure.

4. REFERENCES

- [1] Doyle E.J. *et al.* Progress in the ITER Physics Basis Chapter 2: Plasma Confinement and Transport, 2007 *Nucl. Fusion* **47** S18
- [2] Osborne T.H., Groebner R.J., Lao L.L., Leonard A.W., Maingi R., Miller R.L., Porter G.D., Thomas D.M., and Waltz R.E. 1997 Proc. 24th European Physical Society Conf. on Controlled Fusion and Plasma Physics (Berchtesgaden, Germany) (European Physical Society, Petit-Lancy, 1997) vol 21A p 1101
- [3] Greenwald M. *et al.* 1997 *Nucl. Fusion* **37** 793
- [4] Suttrop W. *et al.* 1997 *Plasma Phys. Control. Fusion* **39** 2051
- [5] Kotschenreuther M., Dorland W., Liu Q.P., Hammett G.W., Beer M.A., Smith S.A., Bondeson A., Cowley S.C. in Fusion Energy 1996 (Proc. 16th Int. Conf. Montreal, 1996), Vol. 2, p. 371, IAEA, Vienna (1997)
- [6] Kinsey J.E., Bateman G., Onjun T., Kritz A.H., Pankin A., Staebler G.M. and Waltz R.E. 2003 *Nucl. Fusion* **43** 1845
- [7] Snyder P.B., Groebner R.J., Leonard, A.W., Osborne T.H., and Wilson H.R. 2009 *Phys. Plasmas* **16** 056118
- [8] Groebner R.J., Leonard, A.W., Snyder, P.B., Osborne, T.O., Maggi, C.F., Fenstermacher, M.E., Petty, C.C. and Owen, L.W. 2009 *Nucl. Fusion* **49** 085037
- [9] Snyder P.B. *et al.* 2009 *Nucl. Fusion* **49** 085035
- [10] Wilson H.R., Snyder P.B., Huysmans G.T.A., and Miller R.L. 2002 *Phys. Plasmas* **9**, 1277
- [11] Snyder P.B., Wilson H.R., Ferron J.R., Lao L.L., Leonard A.W., Osborne T.H., Turnbull A.D., Mossessian D., Murakami M. and Xu X.Q. 2002 *Phys. Plasmas* **9** 2037
- [12] Snyder P.B., Wilson H.R., Ferron J.R., Lao L.L., Leonard A.W., Mossessian D., Murakami M., Osborne T.H., Turnbull A.D. and Xu, X.Q. 2004 *Nucl. Fusion* **44** 320
- [13] Maggi C.F. *et al.* 2010 *Nucl. Fusion* **50** 025023
- [14] Groebner R.J., Osborne T.H., Leonard A.W., and Fenstermacher M.E. 2009 *Nucl. Fusion* **49** 045013
- [15] Osborne T.H., Snyder P.B., Burrell K.H., Evans T.E., Fenstermacher M.E., Leonard A.W., Moyer R.A., Schaffer M.J. and West W.P. 2008 *J. Physics: Conference Series* **123** 012014
- [16] Carlstrom T.N. *et al.*, 1992 *Rev. Sci. Instrum.* **63** 4901
- [17] Gohil P., Burrell K.H., Groebner R.J., Kim J., Martin W.C., McKee E.L. and Seraydarian R.P. 1991 Proc. 14th Symp. on Fusion Engineering (San Diego, California) vol 2., 1992 Inst. of Electrical and Electronics Engineers (New York) 1199

- [18] Lao L.L., St. John H., Stambaugh R.D., Kellman A.G., and Pfeiffer W. 1985 *Nucl. Fusion* **25** 1611
- [19] St. John H. et al. in Plasma Physics and Controlled Nuclear Fusion Research 1994 (Proc. 15th Int. Conf. Seville, 1994), Vol. 3, p.603, IAEA, Vienna (1996)
- [20] Callen J.D., Colchin R.J., Fowler R.H., McAlees D.G. and Rome J.A. in Plasma Physics and Controlled Nuclear Fusion Research 1974 (Proc. 5th Int. Conf. Tokyo, 1974), Vol. I, p. 645, IAEA, Vienna (1975)
- [21] Doyle E.J. et al., "Demonstration of ITER operational scenarios on DIII-D," submitted for publication to *Nucl. Fusion*
- [22] Groebner R.J. et al. 2001 *Nucl. Fusion* **41** 1789
- [23] Rice B.W., Nilson D.G., and Wroblewski D. 1995 *Rev. Sci. Instrum.* **66**, 373
- [24] Sauter O., Angioni C., and Lin-Liu Y.R. 1999 *Phys. Plasmas* **6** 2834
- [25] Sauter O., Angioni C., and Lin-Liu Y.R. 2002 *Phys. Plasmas* **9** 5140
- [26] Snyder P.B. and Hammett G.W. 2001 *Phys. Plasmas* **8** 744
- [27] Jenko F. and Dorland W. 2001 *Plasma Phys. Control. Fusion* **43** A141
- [28] Scott B.D. 2003 *Plasma Phys. Control. Fusion* **45** A385
- [29] Candy J. 2005 *Phys. Plasmas* **12** 072307
- [30] Miller R.L., Lin-Liu Y.R., Turnbull A.D., Chan, V.S., Pearlstein L.D., Sauter O. and Villard L. 1997 *Phys. Plasmas* **4** 1062
- [31] Osborne T.H., Ferron J.R., Groebner R.J., Lao L.L., Leonard A.W., Mahdavi M.A., Maingi R., Miller R.L., Turnbull A.D., Wade M. and Watkins J.G. 2000 *J. Plasma Phys. Control. Fusion* **42** A175
- [32] Wolfrum E., Burckhart A., Fischer R., Hicks N., Konz C., Kurzan B., Langer B., Putterich T., Zohm H. and the ASDEX Upgrade Team 2009 *Plasma Phys. Control. Fusion* **51** 124057
- [33] Wade M.R., Murakami M. and Politzer P.A. 2004 *Phys. Rev. Lett.* **92** 235005
- [34] Thomas D.M., Groebner R.J., Leonard A.W. and Osborne T.H. in Proc. 33rd EPS Conference on Plasma Phys. Rome 2006 ECA volume **30I**, P-5.139

5. ACKNOWLEDGMENT

This work was supported by the US Department of Energy under DE-FC02-04ER54698, DE-FG02-08ER54984, DE-AC05-00OR22725, DE-FG02-89ER53296, DE-FG02-08ER54999, DE-AC52-07NA27344, DE-FG02-07ER54917, and DE-AC04-94AL85000.